Biochemistry
Article
Cite This: Biochemistry XXXX, XXX, XXX−XXX
pubs.acs.org/biochemistry

Crystal Structure of Cucumene Synthase, a Terpenoid Cyclase That Generates a Linear Triquinane Sesquiterpene

Patrick N. Blank,[†,§] Travis A. Pemberton,[†,§] Jeng-Yeong Chow,[‡] C. Dale Poulter,[‡] and David W. Christianson*[,†]

[†]Roy and Diana Vagelos Laboratories, Department of Chemistry, University of Pennsylvania, 231 South 34th Street, Philadelphia, Pennsylvania 19104-6323, United States

[‡]Department of Chemistry, University of Utah, 315 South 1400 East, Salt Lake City, Utah 84112, United States

ABSTRACT: Linear triquinanes are sesquiterpene natural products with hydrocarbon skeletons consisting of three fused five-membered rings. Importantly, several of these compounds exhibit useful anticancer, anti-inflammatory, and antibiotic properties. However, linear triquinanes pose significant challenges to organic synthesis because of the structural and stereochemical complexity of their hydrocarbon skeletons. To illuminate nature's solution to the generation of linear triquinanes, we now describe the crystal structure of *Streptomyces clavuligerus* cucumene synthase. This sesquiterpene cyclase catalyzes the stereospecific cyclization of farnesyl diphosphate to form a linear triquinane product, (5*S*,7*S*,10*R*,11*S*)-cucumene. Specifically, we report the structure of the wild-type enzyme at 3.05 Å resolution and the structure of the T181N variant at 1.96 Å resolution, both in the open active site conformations without any bound ligands. The high-resolution structure of T181N cucumene synthase enables inspection of the active site contour, which adopts a three-dimensional shape complementary to a linear triquinane. Several aromatic residues outline the active site contour and are believed to facilitate cation−π interactions that would stabilize carbocation intermediates in catalysis. Thus, aromatic residues in the active site not only define the template for catalysis but also play a role in reducing activation barriers in the multistep cyclization cascade.

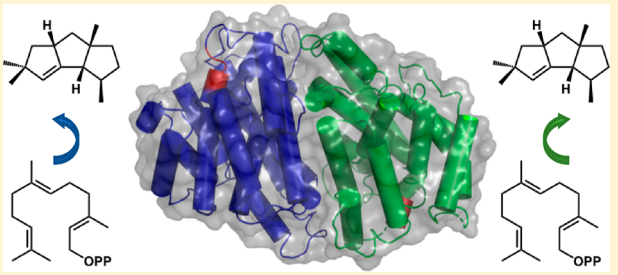

During the past decade, approximately 3000 new terpenoid natural products have been discovered per year, and to date, more than 80000 terpenoids have been identified in all forms of life.[1] Genome mining has accelerated the identification of new terpenoids through the discovery and characterization of new terpenoid cyclases.[2] The catalytic activity of these enzymes underlies exquisite chemodiversity in the hydrocarbon skeletons of all terpenoid natural products.[3−8] The active site contours of terpenoid cyclases function as templates in catalysis. Each template constrains a flexible prenyl diphosphate substrate with a specific conformation that facilitates a specific multistep reaction.[9−13] Active site contours differ from one cyclase to another; different active site contours, i.e., different cyclization templates, direct different reaction sequences.

Class I terpenoid cyclases utilize three Mg^{2+} ions (or sometimes three Mn^{2+} ions) to trigger the ionization of the prenyl diphosphate substrate, resulting in the formation of an allylic cation−inorganic pyrophosphate ion pair.[14] One of the remaining substrate π bonds then reacts with the allylic cation to generate a new carbon−carbon σ bond. The catalytic metal ions initiating this chemistry are coordinated by the aspartate-rich metal ion-binding motif **D**DXX**D** and the NSE/DTE metal ion-binding motif (**N**,**D**)D(L,I,V)X(**S**,**T**)XXX**E** (metal ion ligands are indicated in boldface).[15−18] While these sequence motifs comprise a reliable signature to facilitate the discovery of new terpenoid cyclases, it is generally impossible to predict exactly what product(s) a terpenoid cyclase will generate solely on the basis of an analysis of its amino acid sequence or three-dimensional structure. Such product determination always requires biochemical analysis.

Recently, however, a successful *de novo* prediction of terpenoid cyclase product formation has been reported solely on the basis of an analysis of primary structure and modeling of tertiary structure.[19] Genome mining experiments with *Streptomyces clavuligerus* led to the discovery of a new terpenoid cyclase (Uniprot entry B5GLM7) exhibiting 33% sequence identity with *Streptomyces coelicolor* epi-isozizaene synthase and 27% identity with *Streptomyces exfoliatus* pentalenene synthase. Network analysis using the Structure−Function Linkage Database and generation of a three-dimensional homology model provided a platform for computational studies, leading to the suggestion that B5GLM7 is a sesquiterpene cyclase that generates a linear triquinane hydrocarbon from substrate farnesyl diphosphate (FPP).[19] Subsequent biochemical analysis confirmed that the new linear triquinane (5*S*,7*S*,10*R*,11*S*)-cucumene was the major cyclic sesquiterpene product generated by B5GLM7

Received: August 28, 2018
Revised: October 2, 2018

DOI: 10.1021/acs.biochem.8b00899
Biochemistry XXXX, XXX, XXX−XXX

(Figure 1). Accordingly, this new sesquiterpene cyclase was named cucumene synthase.[19]

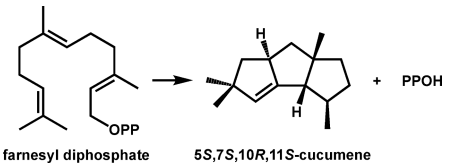

Figure 1. Reaction catalyzed by *S. clavuligerus* cucumene synthase. Abbreviations: OPP, diphosphate; PPOH, inorganic pyrophosphate.

Of the three subfamilies of triquinane natural products—linear triquinanes, angular triquinanes, and propellanes—linear triquinanes such as cucumene have presented critical challenges for synthetic organic chemistry. The synthesis of sesquiterpenes containing multiple fused five-membered rings through multistep reactions has required the development of new synthetic methodology.[20−27] Interest in this family of natural products has also been inspired by the biological activity of certain linear triquinanes. For example, capnellane triquinanes exhibit submicromolar toxicity against leukemia and renal cancer cell lines,[28] and capnellene itself exhibits potent anti-neuroinflammatory and analgesic effects.[29] In another example, hirsutane triquinanes exhibit useful antimicrobial properties,[30,31] and recently identified chondrosterin triquinanes exhibit cytotoxicity against seven different cancer cell lines.[32] Thus, the discovery of cucumene synthase, which generates a linear triquinane in a single enzyme-catalyzed reaction, represents a significant advance for biosynthetic chemistry and the generation of triquinane hydrocarbon skeletons.[19]

To assess the quality of the homology model used to predict the function of cucumene synthase[19] and to provide a foundation for studying terpenoid cyclase structure−function relationships, we now describe crystal structures of wild-type cucumene synthase and T181N cucumene synthase from *S. clavuligerus*. As a sesquiterpene cyclase that catalyzes an anti-Markovnikov C1−C11 cyclization reaction, cucumene synthase is only the second such cyclase to yield a crystal structure (the first anti-Markovnikov cyclase to yield a crystal structure was pentalenene synthase[33]). Comparisons of cucumene synthase with other sesquiterpene cyclases reveal active site features that direct this unusual chemistry, including a productlike active site contour containing aromatic side chains oriented to provide electrostatic stabilization of carbocation intermediates during catalysis through cation−π interactions.

MATERIALS AND METHODS

Expression and Purification. The wild-type cucumene synthase plasmid,[19] comprised of an N-terminal hexahistidine tag with a TEV protease cleavage site, was transformed into *Escherichia coli* BL21 (DE3) RIL cells. Cells were plated on Luria-Bertani (LB) agar and grown overnight. Single colonies were picked and used to inoculate 10 mL starter cultures of LB broth with 500 μM ampicillin and 50 μM chloramphenicol. Starter cultures were grown at 37 °C overnight and subsequently used to inoculate 1 L of LB broth with 500 μM ampicillin and 50 μM chloramphenicol and grown at 37 °C until the OD_{600} reached 0.8. Cultures were then induced with 500 μM isopropyl β-D-1-thiogalactopyranoside for approximately 8 h. Cells were centrifuged for 15 min at 5400*g*. The pellet was collected, flash-frozen, and stored at −80 °C.

Frozen pellets were thawed at room temperature, resuspended in buffer A [20 mM 4-(2-hydroxyethyl)-1-piperazineethanesulfonic acid (HEPES) (pH 8.0), 300 mM NaCl, 5% glycerol], sonicated, and centrifuged for 1 h at 37000*g*. The clarified supernatant was diluted approximately 3-fold with buffer A and run over a 5 mL Ni-NTA column (GE Healthcare). The column was subsequently washed with buffer A containing 30 mM imidazole and then with buffer A containing 300 mM imidazole. Fractions containing cucumene synthase were pooled and treated with 1.0 mL of 1 mg/mL TEV protease. The mixture was dialyzed overnight in a semipermeable membrane (molecular weight cutoff of 10 kDa) against 2 L of buffer A.

The protein sample was centrifuged for approximately 5 min at 5400*g* to remove the precipitate, and a 5 mL Ni-NTA column was loaded with the supernatant. Cucumene synthase exhibited a small degree of nonspecific binding and was eluted with buffer A augmented with 30 mM imidazole. Protein-containing fractions were pooled and loaded onto a Superdex 200 (GE Healthcare) column equilibrated with buffer B [50 mM Tris (pH 7.5), 300 mM NaCl, 5% glycerol, and 0.1 mM tris(2-carboxyethyl)phosphine (TCEP)]. A small amount of soluble aggregate was removed; however, fractions corresponding to the correct molecular weight were collected, and the enzyme was concentrated to approximately 10 mg/mL.

The T181N cucumene synthase variant was prepared by polymerase chain reaction mutagenesis[34] starting with the wild-type cucumene synthase plasmid.[19] This residue was among a group of residues selected for substitution based on their anticipated locations in the active site as suggested by homology modeling. The expression and purification of T181N cucumene synthase followed the same protocol described above for wild-type cucumene synthase. Only this particular variant yielded crystals, but these crystals exhibited superior X-ray diffraction properties.

Crystallization. Wild-type cucumene synthase was crystallized by the vapor diffusion method. Briefly, a 1 μL drop containing 10 mg/mL cucumene synthase, 1.0 mM $MgCl_2$, 2.0 mM sodium pyrophosphate, and 2.0 mM benzyltriethylammonium chloride (BTAC) was added to a 1 μL drop consisting of 0.1 M Bis-Tris (pH 6.0−7.5) and 12−25% PEG 3350 and then equilibrated against a 500 μL reservoir of a precipitant solution. Thin platelike crystals appeared after 1 day at room temperature. These crystals were transferred to a cryoprotectant buffer consisting of 0.1 mM Bis-Tris (pH 7.0), 25% PEG 3350, 1.0 mM $MgCl_2$, 2.0 mM sodium pyrophosphate, 2.0 mM BTAC, and 5−20% ethylene glycol. The concentration of ethylene glycol was initially 5% and then gradually increased by 5% increments to a final concentration of 20%. This gradual transfer was done to preserve the integrity of the crystals, because direct transfer to 20% ethylene glycol solutions caused crystal cracking and resulted in poor diffraction. Finally, crystals were flash-cooled in liquid nitrogen.

The site-specific variant T181N cucumene synthase was similarly crystallized by the vapor diffusion method. Briefly, a 1 μL drop of 10 mg/mL T181N cucumene synthase, 1.0 mM $MgCl_2$, 2 mM sodium pyrophosphate, and 2 mM BTAC was added to a 1 μL drop of 0.1 M Bis-Tris (pH 6.5−8.0) and 12−25% PEG monomethyl ether 5000 and then equilibrated against a 500 μL reservoir of a precipitant solution. Clusters of square rod-shaped crystals appeared after 1 day at room

DOI: 10.1021/acs.biochem.8b00899
Biochemistry XXXX, XXX, XXX−XXX

temperature. Crystals were transferred to a cryoprotectant buffer consisting of 0.1 mM Bis-Tris (pH 7.0), 25% PEG monomethyl ether 5000, 1.0 mM $MgCl_2$, 2.0 mM sodium pyrophosphate, 2.0 mM BTAC, and 5−20% ethylene glycol. The ends of these rod-shaped crystals were snapped off from clusters and flash-cooled in liquid nitrogen.

Data Collection and Refinement. X-ray diffraction data from crystals of wild-type cucumene synthase were collected using beamline 17-ID AMX at the National Synchrotron Light Source (NSLS-II), Brookhaven National Laboratory. Crystals diffracted to 3.05 Å resolution and belonged to monoclinic space group $P2_1$ (a = 63.75 Å, b = 95.85 Å, c = 102.30 Å, α = 90.0°, β = 96.9°, and γ = 90.0°). Data reduction was achieved using XDS[35] and Aimless.[36] The initial electron density map was phased by molecular replacement with Phaser,[37] using the crystal structure of wild-type pentalenene synthase {amino acid sequence identity of 33% [Protein Data Bank (PDB) entry 1PS1]}[33] as a search model. The AutoBuild routine implemented in Phenix[38] was used to fit the electron density map to generate an initial model of cucumene synthase. Several rounds of refinement with routines implemented in Phenix and model rebuilding using Coot[39] yielded a final model with an R_{work} of 0.244 and an R_{free} of 0.299.

Diffraction data from crystals of T181N cucumene synthase were collected using beamline 24-ID-C of the Northeast Collaborative Access Team (NE-CAT) at the Advanced Photon Source, Argonne National Laboratory. Crystals diffracted to 1.96 Å resolution and belonged to orthorhombic space group $P22_12_1$ (a = 58.33 Å, b = 91.81 Å, and c = 124.96 Å). Data reduction was performed with XDS as implemented in Aimless.[35,36] Phaser[37] was used to determine the structure by molecular replacement using the 3.05 Å resolution structure of wild-type cucumene synthase as a search model. The structure was refined using Phenix.[38] Water molecules were built into the electron density map in the later stages of refinement and visualized using Coot.[39] Refinement converged to an R_{work} of 0.174 and an R_{free} of 0.210. All statistics for data collection and crystallographic structure refinement are listed in Table 1. MolProbity was used for analysis and validation of final refined structures.[40]

Product Docking in the Cucumene Synthase Active Site. The (5*S*,7*S*,10*R*,11*S*)-cucumene structure was drawn in a structure editor and converted to a SMILES format string for input into the SMILES Translator and Structure File Generator (https://cactus.nci.nih.gov/translate/), which yielded a coordinate file in .pdb format. To guide the docking of cucumene in the active site of T181N cucumene synthase, the molecular surface of the protein was generated using the surface cavity function in Pymol with a probe radius of 1.6 Å. Cucumene was docked manually in the active site pocket, such that the curvature of the triquinane skeleton matched the natural curvature of the pocket. Computational approaches are available for docking ligands in terpenoid cyclase active sites, e.g., those developed by Jacobson,[41] Major,[42] and Tantillo,[43] but given the productlike active site contour, these approaches were not utilized for product docking. However, computational approaches will be invaluable for future studies of the binding of reaction intermediates.

RESULTS

Structure of Cucumene Synthase. The 3.05 Å resolution structure of wild-type cucumene synthase exhibits the class I terpenoid cyclase fold, which consists of an α-helix bundle

Table 1. Data Collection and Refinement Statistics for Cucumene Synthase

	wild type	T181N
synchrotron	NSLS-II	APS
beamline	17-ID-1; AMX	24-ID-C
detector	EIGER	PILATUS
wavelength (Å)	0.979	0.979
resolution (Å)[a]	29.90−3.05 (3.16−3.05)	62.48−1.96 (2.03−1.96)
total/unique reflections (no.)[a]	79691/23205 (13732/4044)	290219/47590 (19636/3316)
R_{merge}[a]	0.147 (0.672)	0.133 (1.020)
$R_{p.i.m.}$[a,b]	0.093 (0.424)	0.058 (0.468)
$CC_{1/2}$[a,c]	0.995 (0.876)	0.996 (0.547)
$I/\sigma(I)$[a]	5.7 (1.7)	12.9 (3.3)
redundancy[a]	3.4 (3.4)	6.1 (5.9)
completeness (%)[a]	98.6 (92.6)	97.5 (98.0)
R_{work}[a]	0.244 (0.354)	0.174 (0.230)
R_{free}[a]	0.299 (0.407)	0.205 (0.299)
no. of non-hydrogen atoms		
protein	7854	4700
solvent	4	451
average B factor (Å^2)		
macromolecules	63	30
solvent	42	37
root-mean-square deviation from ideal geometry		
bonds (Å)	0.003	0.007
angles (deg)	0.57	0.77
Ramachandran plot (%)[d]		
favored	96.12	98.16
allowed	3.88	1.51
outliers	0.0	0.33
rotamer outliers (%)	1.59	0.64
Clashscore	5.91	5.99
Cβ outliers (%)	0	0
PDB entry	6M7F	6EGK

[a]Values in parentheses refer to data in the highest-resolution shell. [b]$R_{p.i.m.} = \{\sum_{hkl}[1/(N-1)]^{1/2}\sum_i|I_{i,hkl} - \langle I\rangle_{hkl}|\}/\sum_{hkl}\sum_i I_{i,hkl}$, where $\langle I\rangle_{hkl}$ is the average intensity for reflection hkl and N is the number of reflections. [c]Pearson correlation coefficient between random half-data sets. [d]Calculated with MolProbity.

(Figure 2a). Four independent monomers of wild-type cucumene synthase are found in the asymmetric unit. Monomer A and monomer B form a dimer; monomer C and monomer D form a second dimer. Active site orientations in each dimer are antiparallel, with a C2 symmetry axis roughly perpendicular to the α-helix bundles. The quaternary structure of the related sesquiterpene synthase, pentalenene synthase,[33] is defined as dimeric by analysis with the PISA server (http://www.ebi.ac.uk/pdbe/pisa/). In the pentalenene synthase dimer, one active site is oriented approximately 90° away from the other (Figure 2b). However, because pentalenene synthase is observed to be a monomer in solution,[44] its apparent dimeric structure in the crystal may be artifactual.

The overall fold of each cucumene synthase monomer is nearly identical. The root-mean-square (rms) deviations of 176−234 Cα atoms between any two monomers range from 0.21 to 0.57 Å. The AB dimer and CD dimer are also quite similar, with a rms deviation for 412 Cα atoms between each dimer of 0.25 Å. Electron density for each monomer is absent for six to eight residues and 37 residues at the N- and C-

DOI: 10.1021/acs.biochem.8b00899
Biochemistry XXXX, XXX, XXX−XXX

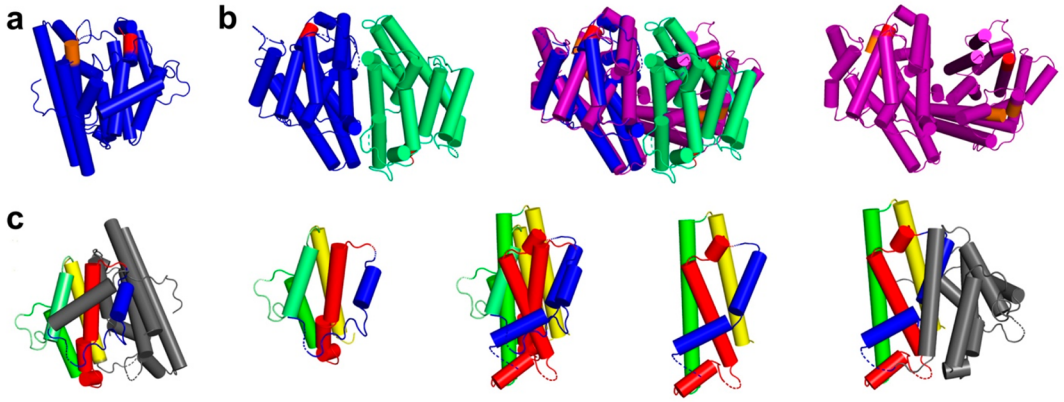

Figure 2. (a) Wild-type cucumene synthase monomer that exhibits the class I terpenoid synthase fold, an α-helix bundle. The locations of metal ion-binding motifs are colored red (aspartate-rich motif) and orange (NSE motif); dashed lines indicate disordered segments. (b) Subunits in the cucumene synthase dimer adopt an antiparallel orientation with *C*2 symmetry (left). This quaternary structure differs from that found in the related dimeric cyclase, pentalenene synthase (right), in which one subunit is rotated approximately 90° away from the other, as evident in the superposition of dimers (center). (c) Four-helix bundles of wild-type cucumene synthase are highlighted as follows: helices C (blue), D (red), E and E′ (green), and F (yellow) at the far left and helices G (blue), H (red), I (green), and J (yellow) at the far right. The remainder of the protein structure is colored gray in each image (the monomer is oriented upside down relative to the monomer orientation in panel a). The respective individual four-helix bundles are more easily viewed after removing the remainder of the protein structure (center left and center right), and these four-helix bundles are aligned as superimposed (center). This topological relationship suggests that the class I terpenoid synthase fold arose from gene duplication and fusion of a four-helix bundle, as first proposed by Huang and colleagues.[46]

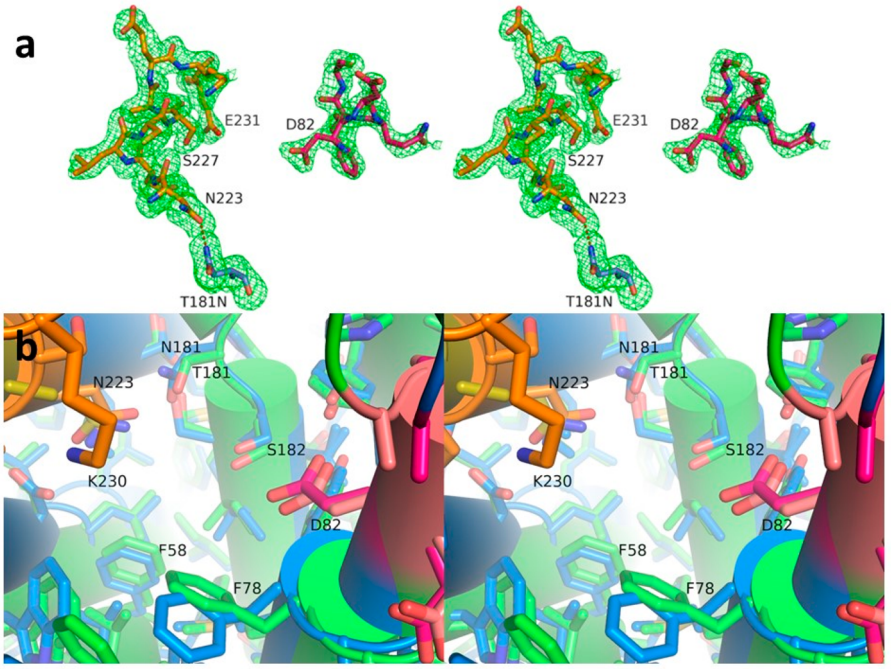

Figure 3. (a) Polder omit map (in stereo) of T181N cucumene synthase (monomer A, contoured at 2.5σ) in which the aspartate-rich motif starting with D82 (magenta backbone), the NSE metal-binding motif starting with N223 (orange backbone), and N181 were omitted from the structure factor calculation. The carboxamide side chain of N181 donates a hydrogen bond to N223 (dashed line). (b) Active site superposition in stereo of wild-type (green with salmon DDXXD motif and gold NSE motif) and T181N (marine with magenta DDXXD motif and orange NSE motif) cucumene synthase, showing that the structures of each are almost identical. Selected residues are labeled; the conformation of F78 is slightly different in each structure.

termini, respectively. Additionally, various loop residues in each monomer are characterized by missing electron density, such that 59, 111, 76, and 117 total residues are missing from monomers A–D, respectively. Missing or weak electron density is likely attributable to molecular disorder and the relatively low resolution.

The active site of cucumene synthase is located within the α-helix bundle, as is typical for class I bacterial cyclases.[8,45] The metal ion-coordinating motifs **D**DXX**D** and (**N**,**D**)D(L,I,V)X-(**S**,**T**)XXX**E** (boldface indicates typical metal ligands) are located at the ends of helices D and H, respectively, at the entrance to the active site. The aspartate-rich motif is ordered in monomers A and B of one dimer but disordered to varying

DOI: 10.1021/acs.biochem.8b00899
Biochemistry XXXX, XXX, XXX–XXX

degrees in monomers C and D; the NSE motif is disordered to varying degrees in all monomers.

The enzyme adopts the open, unliganded active site conformation despite having been crystallized in the presence of Mg^{2+} and inorganic pyrophosphate, which were expected to bind and stabilize the closed active site conformation.[5,8] Least-squares superposition with the homology model of cucumene synthase in the closed conformation initially constructed to predict the triquinane product[19] yields a rms deviation of 2.2 Å (252 Cα atoms). Because rms deviations between open and closed terpenoid cyclase conformations typically range from 1.5 to 2.0 Å, the rms deviation of 2.2 Å obtained for this comparison serves to validate the homology model of cucumene synthase and the computational approach used for its construction.

It has been noted recently that the evolutionary origins of the class I terpenoid synthase fold reside in the primordial gene duplication and fusion of a four-helix bundle protein.[46] This is the case for all class I terpenoid cyclases, including cucumene synthase, in which helices C−F are topologically equivalent to helices G−J, respectively (Figure 2c). The aspartate-rich and NSE metal ion-binding motifs thus reside in topologically identical positions on helices D and H, respectively. Terpenoid synthases of primary metabolism, such as the prenyltransferase farnesyl diphosphate synthase, contain aspartate-rich motifs on helices D and H (i.e., they do not contain NSE motifs). This could suggest that the ancestral four-helix bundle precursor contained an aspartate-rich motif and that this motif persisted after gene duplication and fusion. If so, the NSE motif on helix H in terpenoid cyclases diverged from an aspartate-rich motif during the evolution of secondary (specialized) metabolism.

The 1.96 Å resolution structure of unliganded T181N cucumene synthase crystallized in the open active site conformation reveals an α-helical fold essentially identical to that of wild-type cucumene synthase (rms deviation of 0.37 Å for 277 Cα atoms between monomer B of T181N cucumene synthase and monomer C of the wild-type enzyme). One dimer resides in the asymmetric unit and exhibits a quaternary structure identical to that observed for the wild-type enzyme. The rms deviation for 234 Cα atoms between monomers A and B of the dimer is 0.36 Å. Electron density is absent for six residues at the N-termini of monomers A and B, 33 residues at the C-terminus of monomer A, and 37 residues at the C-terminus of monomer B. Additionally, various loop residues in each monomer are characterized by missing electron density, such that 44 and 51 total residues are missing from monomer A and monomer B, respectively. Given the higher resolution of the T181N cucumene synthase structure, we attribute these missing residues mainly to molecular disorder. We speculate that disordered loops might become ordered after ligand binding, e.g., as found in the related sesquiterpene cyclase epi-isozizaene synthase.[47]

The aspartate-rich motif $D^{82}DQFD$ is ordered in monomer A and disordered in monomer B of T181N cucumene synthase, whereas the NSE motif $N^{223}DLCSAEKE$ is ordered in both monomers (Figure 3a). Molecular disorder for these metal ion-binding motifs is also found in wild-type cucumene synthase, but they are expected to become fully ordered upon metal ion and substrate binding. Protein−metal ion−substrate binding interactions would likely induce a structural transition to a closed active site conformation. Similar substrate-induced conformational transitions have been observed in other bacterial cyclases, e.g., epi-isozizaene synthase.[47] Active site closure protects carbocationic reaction intermediates from premature quenching by solvent molecules.

The T181N substitution appears to be responsible for stabilizing the NSE motif in an ordered conformation, in contrast with the apparent disorder for this motif observed in the structure of wild-type cucumene synthase. The newly introduced N181 side chain forms hydrogen bonds with S183 and N223, the latter of which is part of the NSE metal ion-binding motif on helix H. In turn, the ordering of the NSE motif and the loop segment that follows may explain why T181N cucumene synthase consistently yields higher-quality crystals that diffract to a resolution much higher than that of crystals of the wild-type enzyme. The NSE motif is disordered in some but not all terpenoid cyclase structures determined in the open conformation. Possibly, a comparable mutation in other terpenoid cyclases that are refractory to crystallization might make such cyclases more amenable to crystallization.

Because the structure of T181N cucumene synthase is determined at a resolution much higher than that of the structure of wild-type cucumene synthase, the structure of the former serves as a useful surrogate of the latter for the purpose of structural analysis. With that said, superposition of wild-type and T181N cucumene synthase structures shows that their active sites are essentially identical, so the higher-resolution structure serves to validate the lower-resolution structure (Figure 3b). Regardless, T1281N cucumene synthase is used here for structural comparisons with other bacterial sesquiterpene cyclases. Least-squares superposition of chain A with unliganded wild-type epi-isozizaene synthase (PDB entry 4LTV; 33% sequence identity) yields a rms deviation of 2.9 Å for 220 Cα atoms, whereas superposition with unliganded pentalenene synthase (PDB entry 1PS1; 27% sequence identity) yields a rms deviation of 1.5 Å for 241 Cα atoms. Thus, the three-dimensional structure of cucumene synthase is more similar to the structure of pentalenene synthase despite sharing lower amino acid sequence identity with this sesquiterpene synthase relative.

Structural Inferences on Catalysis. Despite co-crystallization of wild-type and T181N cucumene synthase enzymes with Mg^{2+} and inorganic pyrophosphate, neither structure contains bound ligands. Even so, structures of the unliganded enzymes provide valuable inferences with regard to catalytic function. Hydrophobic residues define the active site contour, including the aromatic side chains of F58, Y77, F78, and W310. These aromatic residues are oriented such that their ring π electrons could provide electrostatic stabilization for carbocation intermediates and the cationic transition states flanking these intermediates. Such interactions have been definitively observed in terpenoid cyclase complexes with quaternary ammonium analogues of carbocation intermediates,[47,48] and the contribution of aromatic residues to catalytic efficiency and cyclization specificity has been probed by mutagenesis of the related cyclase epi-isozizaene synthase.[47,49,50] Density functional theory calculations by Hong and Tantillo show that active site aromatic residues in terpenoid cyclases may interact with C−H bonds hyperconjugated with adjacent carbocations to form C−H···π interactions.[51,52]

Using the high-resolution structure of T181N cucumene synthase, we generated a molecular contour of the enzyme active site and manually docked cucumene into this contour. The curvature of the triquinane skeleton of cucumene appears to match the natural curvature of the active site pocket (Figure

DOI: 10.1021/acs.biochem.8b00899
Biochemistry XXXX, XXX, XXX−XXX

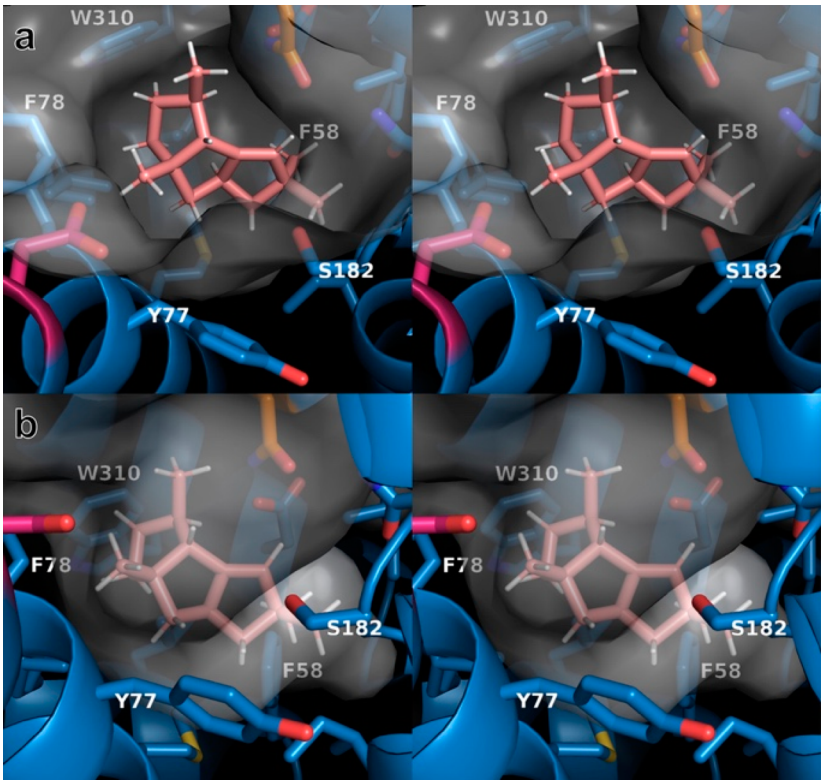

Figure 4. (a) Stereoview of a plausible model of (5*S*,7*S*,10*R*,11*S*)-cucumene (C, salmon; H, white) complexed in the active site pocket of T181N cucumene synthase. For reference, the aspartate-rich (red) and NSE (orange) motifs are indicated. (b) Same as panel a, but a side-on view. The active site opens to the top of the figure. Selected active site residues are labeled.

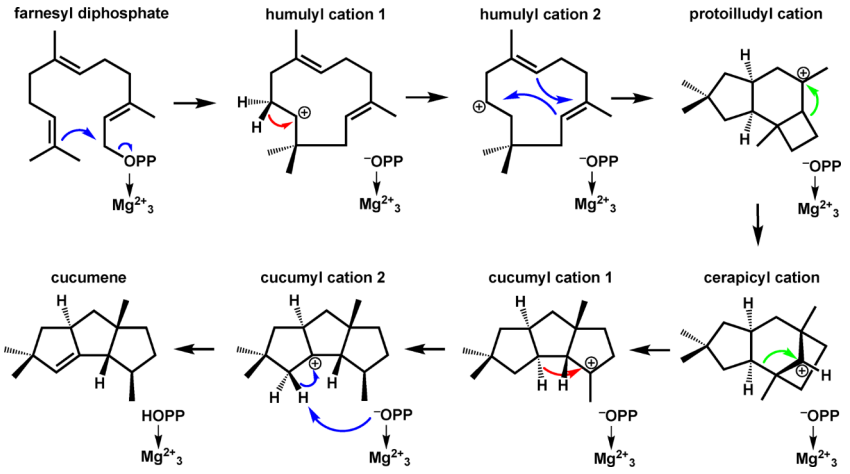

Figure 5. Proposed mechanism of cucumene synthase. Red arrows indicate 1,2- or 1,3-hydride transfers, and green arrows indicate 1,2-alkyl migrations. PPO represents diphosphate, and ⁻OPP and PPOH represent different protonation states of inorganic pyrophosphate.

4). As mentioned above, aromatic residues defining the contour are poised for interactions with carbocation intermediates. Additionally, the backbone carbonyl of A180 at the helix G break may also provide electrostatic stabilization of cationic intermediates through charge-dipole interactions. The helix G break is common to class I terpenoid synthases; the possible catalytic importance of the backbone carbonyl group exposed at the break was first noted by Pandit and colleagues[53] and further explored by Dickschat and colleagues.[54,55]

The experimentally determined crystal structure of cucumene synthase and the model of the enzyme−product complex serve as a platform for understanding the chemical mechanism of triquinane formation. A proposed mechanism of cucumene synthase is outlined in Figure 5. This mechanism shares several identical features with that proposed for pentalenene synthase, which similarly catalyzes an initial C1−C11 macrocyclization reaction.[56−59] Related mechanisms have also been computed using the Artificial Force Induced Reaction method.[60] First, ionization of the substrate diphosphate group is triggered by coordination to the Mg^{2+}_3 cluster. Elegant quantum chemical studies of the pentalenene synthase reaction indicate that C1−C11 bond formation occurs in a concerted fashion with C1−O bond dissociation, leading directly to humulyl cation 1,[56] a

DOI: 10.1021/acs.biochem.8b00899
Biochemistry XXXX, XXX, XXX−XXX

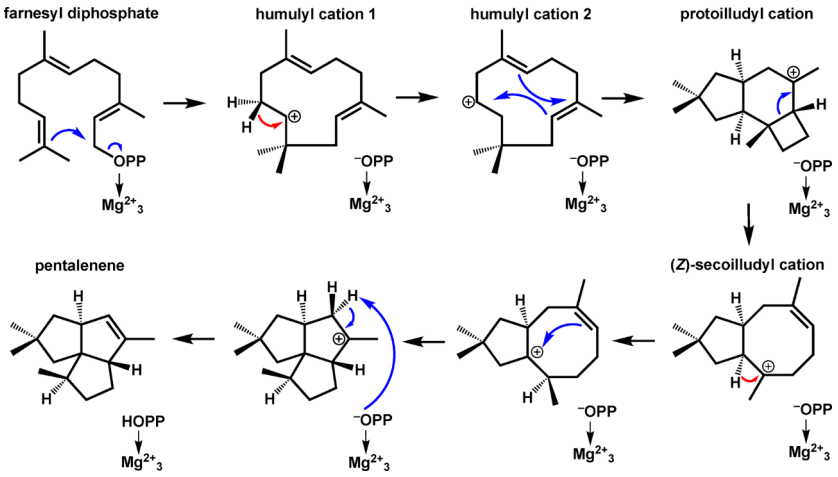

Figure 6. Proposed mechanism of pentalenene synthase. This mechanism reflects the most recent details emanating from experimental and computational studies.[56−59] Red arrows indicate 1,2-hydride transfers. PPO represents diphosphate, and ⁻OPP and PPOH represent different protonation states of inorganic pyrophosphate.

common intermediate in sesquiterpene biosynthesis.[58] Humulyl cation 2 subsequently results from a 1,2-hydride shift and then undergoes a concerted reaction to yield two new carbon−carbon bonds, forming the tricyclic protoilludyl cation intermediate with a 5−6−4 ring structure. This intermediate has been confirmed in the pentalenene synthase mechanism through kinetic isotope effects using an isotopically labeled substrate;[57] similarly, we advance that the protoilludyl cation is an intermediate in the cucumene synthase reaction.[19]

Following formation of the protoilludyl cation, tandem 1,2-alkyl migrations are proposed to generate the triquinane skeleton.[13] The first alkyl migration converts the protoilludyl cation into the cerapicyl cation, and the second alkyl migration yields cucumyl cation 1 with a 5−5−5 ring structure. We suggest that a 1,3-hydride transfer follows to form cucumyl cation 2, and then a final proton elimination yields cucumene. Because the proton elimination and hydride transfer occur on opposite sides of the 5−5−5 ring system, it is possible that these steps could occur in a concerted fashion. We speculate that the co-product, inorganic pyrophosphate, is the general base that quenches the final carbocation intermediate. We note that an alternative biosynthetic pathway has been suggested that leads from humulyl cation 1 to the protoilludyl cation through a bicyclic cation with a 5−8 ring structure.[13,61] However, this proposed pathway does not accommodate the *trans*−*cis* isomerization of a C═C bond in humulene that is required to form the bicyclic cation.

Active Site Contours of Cucumene Synthase and Pentalenene Synthase. Among sesquiterpene cyclases that catalyze initial anti-Markovnikov C1−C11 cyclization reactions, only cucumene synthase and pentalenene synthase have yielded X-ray crystal structures. Both of these cyclases share a common mechanism through the formation of the protoilludyl cation; however, the mechanisms subsequently diverge, with cucumene synthase generating a linear triquinane product (Figure 5) and pentalenene synthase generating an angular triquinane product (Figure 6) Even so, the active site contours of these enzymes share features that facilitate the shared chemistry of initial C1−C11 cyclization and protoilludyl cation formation.

The four aromatic residues defining much of the active site surface contour of cucumene synthase, F58, Y77, F78, and W310, align with F57, F76, F77, and W308, respectively, in the pentalenene synthase active site. Each corresponding pair of residues adopts similar conformations except for the third pair: F78 of cucumene synthase and F77 of pentalenene synthase (Figure 7).

Most other residues defining the active site contour of each enzyme are similar, with two notable exceptions. First, D307 of cucumene synthase corresponds to S305 of pentalenene synthase, and their side chain conformations differ substantially. Parenthetically, we note that it is unusual to find a negatively charged carboxylate side chain in the active site of a terpenoid cyclase; however, the side chain of D307 does not protrude into the active site because of its hydrogen bond with S222. Second, L303 of cucumene synthase corresponds to V301 in pentalenene synthase, and their side chain conformations differ substantially. The overall result of structural differences with these three pairs of corresponding residues is an elongated active site contour in cucumene synthase and a wider, more triangular-shaped active site contour in pentalenene synthase (Figure 7). Thus, each active site contour adopts a productlike shape similar to that of its respective triquinane product, yet the common features of these contours, defined by the conserved residues and residue conformations in each active site, presumably enable the initial anti-Markovnikov C1−C11 cyclization reaction and formation of the common protoilludyl cation intermediate.

Although comparisons of cucumene synthase and pentalenene synthase are restricted to crystal structures of their unliganded conformations, the active site contours of terpenoid cyclases in their open and closed conformations can be quite similar, as first demonstrated for aristolochene synthase.[62] Thus, just as a productlike active site contour would be expected for the closed conformations of cucumene synthase and pentalenene synthase, many features of the productlike contour are preserved in their open conformations.

■ CONCLUDING REMARKS

Crystal structures of wild-type cucumene synthase and T181N cucumene synthase provide the first insight into how a linear triquinane sesquiterpene is generated from farnesyl diphosphate in an enzyme-catalyzed reaction. The active site contour functions as a template for catalysis and is quite comple-

DOI: 10.1021/acs.biochem.8b00899
Biochemistry XXXX, XXX, XXX−XXX

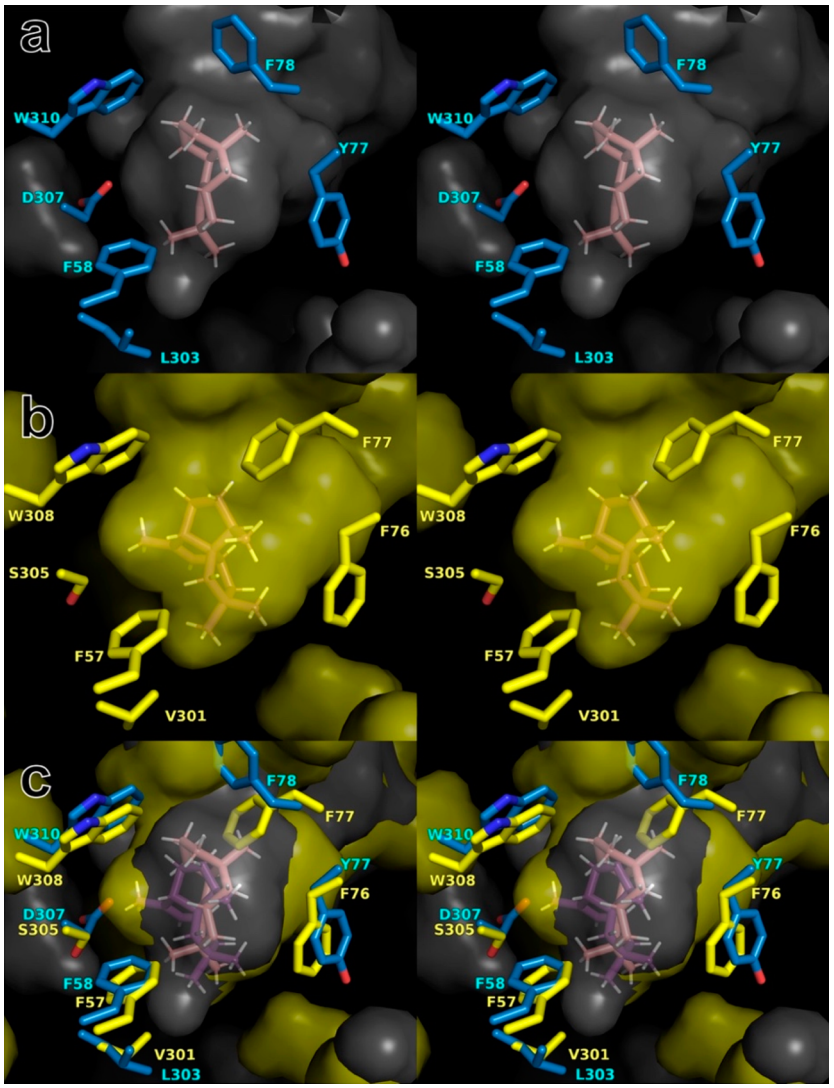

Figure 7. (a) Stereoview of T181N cucumene synthase complexed with cucumene (C, salmon; H, white) (same as in Figure 4, but a different orientation). (b) Stereoview of wild-type pentalenene synthase (PDB entry 1PS1) complexed with pentalenene (C, purple; H, white). (c) Stereoview of the aligned active sites of cucumene synthase (gray) and pentalenene synthase (yellow), highlighting aromatic residues common to both active sites. Modeled product orientations are such that the final deprotonation steps yielding these products could be mediated by the co-product, inorganic pyrophosphate (not shown).

mentary in shape to that of the specific stereoisomer, (5*S*,7*S*,10*R*,11*S*)-cucumene, generated by the enzyme. This productlike template constrains the substrate conformation to ensure that the correct sequence of bond forming reactions follows metal ion-triggered substrate ionization.

The active site template enforces only the precatalytic substrate conformation that leads to initial C1−C11 bond formation and prevents conformations that would lead to initial C1−C10 or C1−C6 cyclization. Curiously, initial C1−C11 cyclization leads to the generation of a secondary carbocation intermediate, the humulyl cation, whereas alternative C1−C10 bond formation would lead to a tertiary carbocation intermediate, which would be energetically more favorable than a secondary carbocation intermediate. Thus, the cucumene synthase active site must play a decisive role in directing the anti-Markovnikov cyclization reaction, both by serving as a rigid template and by providing preferential stabilization for the less stable secondary carbocation intermediate. Aromatic residues defining the active site contour likely engage in cation−π interactions to stabilize carbocation intermediates. Thus, aromatic residues not only comprise an important part of the catalytic template but also provide a means to stabilize otherwise unfavorable cationic intermediates and the transition states leading to and away from these intermediates. Future studies will allow us to test this mechanism in greater detail.

■ ASSOCIATED CONTENT

Accession Codes

The atomic coordinates and crystallographic structure factors of wild-type and T181N cucumene synthase have been deposited in the Protein Data Bank as entries 6M7F and 6EGK, respectively.

■ AUTHOR INFORMATION

Corresponding Author

*Telephone: 215-898-5714. E-mail: chris@sas.upenn.edu.

ORCID

C. Dale Poulter: 0000-0001-7682-3095

DOI: 10.1021/acs.biochem.8b00899
Biochemistry XXXX, XXX, XXX−XXX

David W. Christianson: 0000-0002-0194-5212

Author Contributions

§P.N.B. and T.A.P. contributed equally to this work.

Funding

The authors thank the National Institutes of Health for Grants GM56838 (D.W.C.) and GM25521 (C.D.P.) in support of this research. J.-Y.C. was supported by an Agency for Science, Technology and Research International Fellowship, Singapore.

Notes

The authors declare no competing financial interest.

■ ACKNOWLEDGMENTS

The authors thank Dr. Stephen Shinsky for helpful scientific discussions and Drs. Matt Jacobson and Bo-Xue Tian for sharing coordinates of the homology model of cucumene synthase constructed using computational approaches as described in ref 19. Additionally, the authors are grateful for access to synchrotron X-ray data collection facilities: the Northeastern Collaborative Access Team beamlines (supported by Grants P1 GM103403 and S10 RR02905) at the Advanced Photon Source, a U.S. Department of Energy (DOE) Office of Science User Facility operated for the DOE Office of Science by Argonne National Laboratory under Contract DE-AC02-06CH11357, and the AMX beamline at the National Synchrotron Light Source II, a DOE Office of Science User Facility operated for the DOE Office of Science by Brookhaven National Laboratory under Contract DE-SC0012704.

■ REFERENCES

(1) Dictionary of Natural Products. http://dnp.chemnetbase.com.
(2) Cane, D. E., and Ikeda, H. (2012) Exploration and mining of the bacterial terpenome. *Acc. Chem. Res. 45*, 463−472.
(3) Cane, D. E. (1990) Enzymatic formation of sesquiterpenes. *Chem. Rev. 90*, 1089−1103.
(4) Davis, E. M., and Croteau, R. (2000) Cyclization enzymes in the biosynthesis of monoterpenes, sesquiterpenes, and diterpenes. *Biosynthesis: Aromatic polyketides, isoprenoids, alkaloids (Vol. 209)*, pp 53−95, Springer-Verlag, Berlin.
(5) Christianson, D. W. (2006) Structural biology and chemistry of the terpenoid cyclases. *Chem. Rev. 106*, 3412−3442.
(6) Christianson, D. W. (2008) Unearthing the roots of the terpenome. *Curr. Opin. Chem. Biol. 12*, 141−150.
(7) Bohlmann, J. (2011) Terpenoid synthases − from chemical ecology and forest fires to biofuels and bioproducts. *Structure 19*, 1730−1731.
(8) Christianson, D. W. (2017) Structural and chemical biology of terpenoid cyclases. *Chem. Rev. 117*, 11570−11648.
(9) Gao, Y., Honzatko, R. B., and Peters, R. J. (2012) Terpenoid synthase structures: a so far incomplete view of complex catalysis. *Nat. Prod. Rep. 29*, 1153−1175.
(10) Miller, D. J., and Allemann, R. K. (2012) Sesquiterpene synthases: passive catalysts or active players? *Nat. Prod. Rep. 29*, 60−71.
(11) Austin, M. B., O'Maille, P. E., and Noel, J. P. (2008) Evolving biosynthetic tangos negotiate mechanistic landscapes. *Nat. Chem. Biol. 4*, 217−222.
(12) Tholl, D. (2006) Terpene synthases and the regulation, diversity and biological roles of terpene metabolism. *Curr. Opin. Plant Biol. 9*, 297−304.
(13) Quin, M. B., Flynn, C. M., and Schmidt-Dannert, C. (2014) Traversing the fungal terpenome. *Nat. Prod. Rep. 31*, 1449−1473.
(14) Aaron, J. A., and Christianson, D. W. (2010) Trinuclear metal clusters in catalysis by terpenoid synthases. *Pure Appl. Chem. 82*, 1585−1597.
(15) Ashby, M. N., and Edwards, P. A. (1990) Elucidation of the deficiency in two yeast coenzyme Q mutants: characterization of the structural gene encoding hexaprenyl pyrophosphate synthetase. *J. Biol. Chem. 265*, 13157−13164.
(16) Ashby, M. N., Kutsunai, S. Y., Ackerman, S., Tzagoloff, A., and Edwards, P. A. (1992) *COQ2* is a candidate for the structural gene encoding *para*-hydroxybenzoate:polyprenyltransferase. *J. Biol. Chem. 267*, 4128−4136.
(17) Cane, D. E., and Kang, I. (2000) Aristolochene synthase: purification, molecular cloning, high-level expression in *Escherichia coli*, and characterization of the *Aspergillus terreus* cyclase. *Arch. Biochem. Biophys. 376*, 354−364.
(18) Rynkiewicz, M. J., Cane, D. E., and Christianson, D. W. (2001) Structure of trichodiene synthase from *Fusarium sporotrichioides* provides mechanistic inferences on the terpene cyclization cascade. *Proc. Natl. Acad. Sci. U. S. A. 98*, 13543−13548.
(19) Chow, J.-Y., Tian, B.-X., Ramamoorthy, G., Hillerich, B. S., Seidel, R. D., Almo, S. C., Jacobson, M. P., and Poulter, C. D. (2015) Computational-guided discovery and characterization of a sesquiterpene synthase from *Streptomyces clavuligerus*. *Proc. Natl. Acad. Sci. U. S. A. 112*, 5661−5666.
(20) Nozoe, S., Furukawa, J., Sankawa, U., and Shibata, S. (1976) Isolation, structure and synthesis of hirsutene, a precursor hydrocarbon of coriolin biosynthesis. *Tetrahedron Lett. 17*, 195−198.
(21) Curran, D. P., and Rakiewicz, D. M. (1985) Tandem radical approach to linear condensed cyclopentanoids. Total synthesis of (±)-hirsutene. *J. Am. Chem. Soc. 107*, 1448−1449.
(22) Mizuno, H., Domon, K., Masuya, K., Tanino, K., and Kuwajima, I. (1999) Total synthesis of (−)-coriolin. *J. Org. Chem. 64*, 2648−2656.
(23) Geng, F., Liu, J., and Paquette, L. A. (2002) Three-component coupling via the squarate ester cascade as a concise route to the bioactive triquinane sesquiterpene hypnophilin. *Org. Lett. 4*, 71−73.
(24) Dhimane, A. L., Aïssa, C., and Malacria, M. (2002) Transannular radical cascade as an approach to the diastereoselective synthesis of linear triquinane. *Angew. Chem., Int. Ed. 41*, 3284−3287.
(25) Jiao, L., Yuan, C., and Yu, Z. X. (2008) Tandem Rh(I)-catalyzed [(5 + 2)+1] cycloaddition/aldol reaction for the construction of linear triquinane skeleton: total syntheses of (±)-1-desoxyhypnophilin. *J. Am. Chem. Soc. 130*, 4421−4430.
(26) Shen, S. J., and Li, W. D. (2013) Formal homoiodo allylsilane annulations: dual total syntheses of (±)-hirsutene and (±)-capnellene. *J. Org. Chem. 78*, 7112−7120.
(27) Nagaraju, C., and Prasad, K. R. (2014) An unusual ring-contraction/rearrangement sequence for making functionalized di- and triquinanes. *Angew. Chem., Int. Ed. 53*, 10997−11000.
(28) Morris, L. A., Jaspars, M., Adamson, K., Woods, S., and Wallace, H. M. (1998) The capnellenes revisited: new structures and new biological activity. *Tetrahedron 54*, 12953−12958.
(29) Jean, Y.-H., Chen, W.-F., Sung, C.-S., Duh, C.-Y., Huang, S.-Y., Lin, C.-S., Tai, M.-H., Tzeng, S.-F., and Wen, Z.-H. (2009) Capnellene, a natural marine compound derived from soft coral, attenuates chronic constriction injury-induced neuropathic pain in rats. *Br. J. Pharmacol. 158*, 713−725.
(30) Takeuchi, T., Iinuma, H., Iwanaga, J., Takahashi, S., Takita, T., and Umezawa, H. (1969) Coriolin, a new basidiomycetes antibiotic. *J. Antibiot. 22*, 215−217.
(31) Abate, D., and Abraham, W.-R. (1994) Antimicrobial metabolites from *Lentinus crinitus*. *J. Antibiot. 47*, 1348−1350.
(32) Huang, L., Lan, W.-J., Deng, R., Feng, G. K., Xu, Q.-Y., Hu, Z.-Y., Zhu, X.-F., and Li, H.-J. (2016) Additional new cytotoxic triquinane-type sesquiterpenoids chondrosterins K−M from the marine fungus *Chondrostereum* sp. *Mar. Drugs 14*, 157.
(33) Lesburg, C. A., Zhai, G., Cane, D. E., and Christianson, D. W. (1997) Crystal structure of pentalenene synthase: mechanistic insights on terpenoid cyclization reactions in biology. *Science 277*, 1820−1824.

DOI: 10.1021/acs.biochem.8b00899
Biochemistry XXXX, XXX, XXX−XXX

(34) Braman, J., Papworth, C., and Greener, A. (1996) Site-directed mutagenesis using double-stranded plasmid DNA templates. *Methods Mol. Biol. 57*, 31−44.
(35) Kabsch, W. (2010) XDS. *Acta Crystallogr., Sect. D: Biol. Crystallogr. 66*, 125−132.
(36) Evans, P. R., and Murshudov, G. N. (2013) How good are my data and what is the resolution? *Acta Crystallogr., Sect. D: Biol. Crystallogr. 69*, 1204−1214.
(37) McCoy, A. J., Grosse-Kunstleve, R. W., Adams, P. D., Winn, M. D., Storoni, L. C., and Read, R. J. (2007) Phaser crystallographic software. *J. Appl. Crystallogr. 40*, 658−674.
(38) Adams, P. D., Afonine, P. V., Bunkóczi, G., Chen, V. B., Davis, I. W., Echols, N., Headd, J. J., Hung, L.-W., Kapral, G. J., Grosse-Kunstleve, R. W., McCoy, A. J., Moriarty, N. W., Oeffner, R., Read, R. J., Richardson, D. C., Richardson, J. S., Terwilliger, T. C., and Zwart, P. H. (2010) *PHENIX*: A comprehensive Python-based system for macromolecular structure solution. *Acta Crystallogr., Sect. D: Biol. Crystallogr. 66*, 213−221.
(39) Emsley, P., Lohkamp, B., Scott, W. G., and Cowtan, K. (2010) Features and development of Coot. *Acta Crystallogr., Sect. D: Biol. Crystallogr. 66*, 486−501.
(40) Chen, V. B., Arendall, W. B., III, Headd, J. J., Keedy, D. A., Immormino, R. M., Kapral, G. J., Murray, L. W., Richardson, J. S., and Richardson, D. C. (2010) MolProbity: all-atom structure validation for macromolecular crystallography. *Acta Crystallogr., Sect. D: Biol. Crystallogr. 66*, 12−21.
(41) Tian, B.-X., Wallrapp, F. H., Holiday, G. L., Chow, J.-Y., Babbitt, P. C., Poulter, C. D., and Jacobson, M. P. (2014) Predicting the functions and specificity of triterpenoid synthases: a mechanism-based multi-intermediate docking approach. *PLoS Comput. Biol. 10*, No. e1003874.
(42) Dixit, M., Weitman, M., Gao, J., and Major, D. T. (2017) Chemical control in the battle against fidelity in promiscuous natural product biosynthesis: the case of trichodiene synthase. *ACS Catal. 7*, 812−818.
(43) O'Brien, T. E., Bertolani, S. J., Zhang, Y., Siegel, J. B., and Tantillo, D. J. (2018) Predicting productive binding modes for substrates and carbocation intermediates in terpene synthases − bornyl diphosphate synthase as a representative case. *ACS Catal. 8*, 3322−3330.
(44) Cane, D. E., Sohng, J.-K., Lamberson, C. R., Rudnicki, S. M., Wu, Z., Lloyd, M. D., Oliver, J. S., and Hubbard, B. R. (1994) Pentalenene synthase. Purification, molecular cloning, sequencing, and high-level expression in *Escherichia coli* of a terpenoid cyclase from *Streptomyces* UC5319. *Biochemistry 33*, 5846−5857.
(45) Chen, M., Harris, G. G., Pemberton, T. A., and Christianson, D. W. (2016) Multi-domain terpenoid cyclase architecture and prospects for proximity in bifunctional catalysis. *Curr. Opin. Struct. Biol. 41*, 27−37.
(46) Huang, H., Levin, E. J., Liu, S., Bai, Y., Lockless, S. W., and Zhou, M. (2014) Structure of a membrane-embedded prenyltransferase homologous to UBIAD1. *PLoS Biol. 12*, No. e1001911.
(47) Aaron, J. A., Lin, X., Cane, D. E., and Christianson, D. W. (2010) Structure of *epi*-isozizaene synthase from *Streptomyces coelicolor* A3(2), a platform for new terpenoid cyclization templates. *Biochemistry 49*, 1787−1797.
(48) Chen, M., Al-lami, N., Janvier, M., D'Antonio, E. L., Faraldos, J. A., Cane, D. E., Allemann, R. K., and Christianson, D. W. (2013) Mechanistic insights from the binding of substrate and carbocation intermediate analogues to aristolochene synthase. *Biochemistry 52*, 5441−5453.
(49) Li, R., Chou, W. K. W., Himmelberger, J. A., Litwin, K. M., Harris, G. G., Cane, D. E., and Christianson, D. W. (2014) Reprogramming the chemodiversity of terpenoid cyclization by remolding the active site contour of *epi*-isozizaene synthase. *Biochemistry 53*, 1155−1168.
(50) Blank, P. N., Barrow, G. H., Chou, W. K. W., Duan, L., Cane, D. E., and Christianson, D. W. (2017) Substitution of aromatic residues with polar residues in the active site pocket of *epi*-isozizaene synthase leads to the generation of new cyclic sesquiterpenes. *Biochemistry 56*, 5798−5811.
(51) Hong, Y. J., and Tantillo, D. J. (2013) C−H···π interactions as modulators of carbocation structure − implications for terpene biosynthesis. *Chem. Sci. 4*, 2512−2518.
(52) Hong, Y. J., and Tantillo, D. J. (2015) Tension between internal and external modes of stabilization in carbocations relevant to terpene biosynthesis: modulating minima depth via C−H···π interactions. *Org. Lett. 17*, 5388−5391.
(53) Pandit, J., Danley, D. E., Schulte, G. K., Mazzalupo, S., Pauly, T. A., Hayward, C. M., Hamanaka, E. S., Thompson, J. F., and Harwood, H. J., Jr. (2000) Crystal structure of human squalene synthase: a key enzyme in cholesterol biosynthesis. *J. Biol. Chem. 275*, 30610−30617.
(54) Baer, P., Rabe, P., Citron, C. A., de Oliveira Mann, C. C., Kaufmann, N., Groll, M., and Dickschat, J. S. (2014) Hedycaryol synthase in complex with nerolidol reveals terpene cyclase mechanism. *ChemBioChem 15*, 213−216.
(55) Baer, P., Rabe, P., Fischer, K., Citron, C. A., Klapschinski, T. A., Groll, M., and Dickschat, J. S. (2014) Induced-fit mechanism in class I terpene cyclases. *Angew. Chem., Int. Ed. 53*, 7652−7656.
(56) Gutta, P., and Tantillo, D. J. (2006) Theoretical studies on farnesyl cation cyclization: pathways to pentalenene. *J. Am. Chem. Soc. 128*, 6172−6179.
(57) Zu, L., Xu, M., Lodewyk, M. W., Cane, D. E., Peters, R. J., and Tantillo, D. J. (2012) Effects of isotopically sensitive branching on product distribution for pentalenene synthase: support for a mechanism predicted by quantum chemistry. *J. Am. Chem. Soc. 134*, 11369−11371.
(58) Hamlin, T. A., Hamann, C. S., and Tantillo, D. J. (2015) Delocalization of charge and electron density in the humulyl cation − implications for terpene biosynthesis. *J. Org. Chem. 80*, 4046−4053.
(59) Lodewyk, M. W., Willenbring, D., and Tantillo, D. J. (2014) Pentalenene formation mechanisms redux. *Org. Biomol. Chem. 12*, 887−894.
(60) Isegawa, M., Maeda, S., Tantillo, D. J., and Morokuma, K. (2014) Predicting pathways for terpene formation from first principles − routes to known and new sesquiterpenes. *Chem. Sci. 5*, 1555−1560.
(61) Schmidt-Dannert, C. (2014) Biosynthesis of terpenoid natural products in fungi. *Adv. Biochem. Eng./Biotechnol. 148*, 19−61.
(62) Shishova, E. Y., Di Costanzo, L., Cane, D. E., and Christianson, D. W. (2007) X-ray crystal structure of aristolochene synthase from *Aspergillus terreus* and evolution of templates for the cyclization of farnesyl diphosphate. *Biochemistry 46*, 1941−1951.

DOI: 10.1021/acs.biochem.8b00899
Biochemistry XXXX, XXX, XXX−XXX